Excitonic Processes in Aromatic Microcrystallites and Bulk Exciton Bandwidths

1997

Yoshitaka Oeda

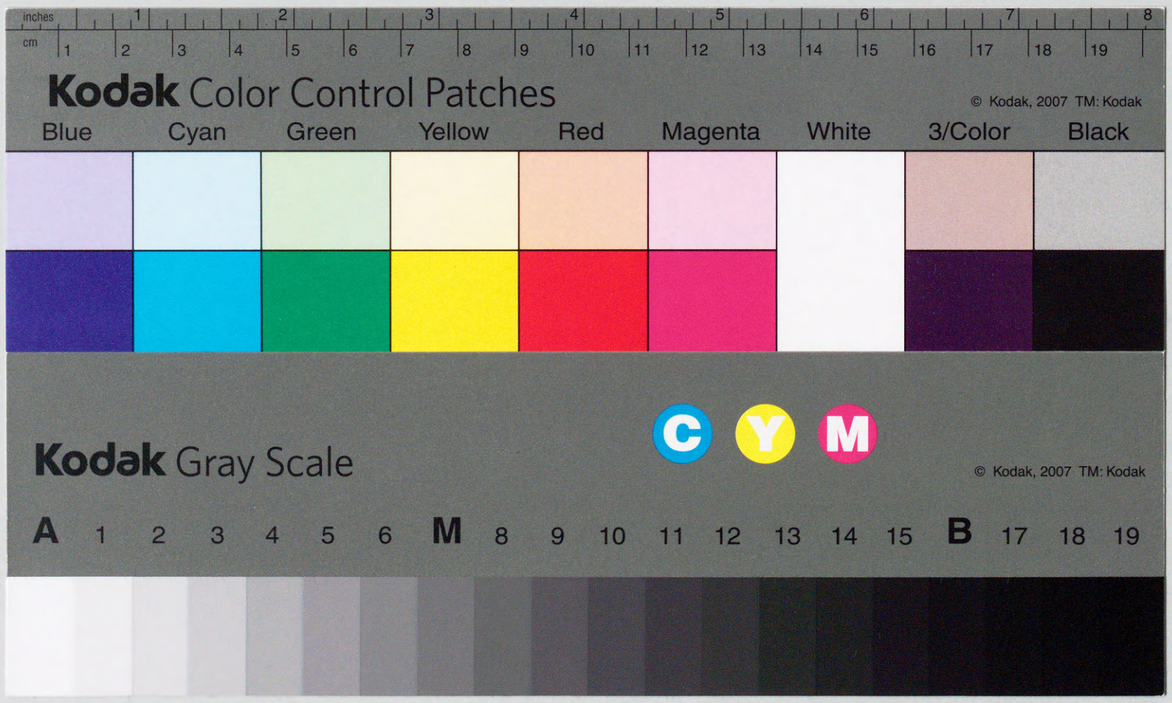

ABSTRACT

A novel experimental method, based on the technology to determine the singlet lowest exciton bandwidth in molecular crystals is reported here. In this method the analysis of the excitation spectrum in microcrystallites is used as a key tool to determine the exciton bandwidth. Analyzing the excitation spectra of pyrene microcrystallites at 2K, we have found that the lowest ^1L_b singlet exciton bandwidth increases superlinearly with microcrystallite size toward a maximum value of 330 cm^{-1}, which is interpreted to be the bandwidth of the lowest exciton band (^1L_b band) in the bulk crystal.

The bandwidth of the bulk crystal thus obtained is discussed in connection with the Davydov splitting of only 15 cm^{-1}. The bandwidths in small microcrystallites are interpreted in terms of the energy separation calculated by the Frenkel exciton theory. Using the bandwidth obtained for bulk pyrene crystal and exciton-phonon coupling constant, the lattice relaxation energy for the ^1L_b exciton has been estimated to be 180 cm^{-1} and the self-trap depth for the V state to be 15 cm^{-1}.

We have found that the k selection rule for the exciton creation is not applicable in small size pyrene microcrystallites, but it is applicable to microcrystallites larger than 50 Å. Comparing the exciton bandwidth in pyrene and anthracene microcrystallites, it is found that the exciton surface scattering does not occur in pyrene microcrystallites but it occurs strongly in anthracene microcrystallites. The surface scattering layer thickness in anthracene microcrystallites is found to be 30 Å.

ACKNOWLEDGMENTS

I am very much indebted to my supervisor Prof. A. H. Matsui for his guidance and valuable discussions during the whole period of this research. I am also deeply indebted to Prof. K. Mizuno for his help in the experimental work, valuable discussions and advice. I would like to thank Dr. M. Takeshima for valuable discussions about the theoretical treatment and comments in furnishing this manuscript. Electron microscope observation on microcrystallite size by Prof. M. Michinomae is greatly acknowledged. I wish to thank Prof. K. Seki (Nagoya University) for information on electron affinities and ionization energies of organic solids used in this work. I am also deeply indebted to Prof. J. Singh (Northern Territory University) for his important comments. Thanks also goes to Mr. Y. Matsushima and Mr. O. Nishi for their assistance in optical measurements. I am pleased to express my gratitude to Mr. T. Higaki, Mr. T. Murase and Dr. S. Okushima for their continued encouragement during the course of this work, and for the financial support by Oji Paper Co., Ltd. The Grant-in-Aid for the new program from the Ministry of Education, Sports and Culture is also gratefully acknowledged.

LIST OF PUBLICATION (Yoshitaka Oeda)

1) Exciton Band Structure of Crystalline Anthracene

A. Matsui, K. Tomioka, Y. Oeda and T. Tomotika

Surface Science, **37** (1973) 849-854.

2) Density of States and the Exciton Band Structure in Crystalline Anthracene

A. Matsui and Y. Oeda

Proceedings of the 6th Molecular Crystal Symposium, Klais (1973) 41-44.

3) An Experimental Approach to Determine the Density of States of an Exciton Band from Thermoabsorption Spectra

A. Matsui, K. Tomioka and Y. Oeda

Memories of Konan Univ. Science Series **16** (1973) 13-19.

4) Dynamical Behavior of Excitons in Crystalline Anthracene and Phenanthrene

K. Tomioka, A. Matsui, H. Amimoto and Y. Oeda

Memories of Konan Univ. Science Series **17** (1974) 1-22.

5) Densities of States of the ^1L_b Exciton Band and Luminescence Processes in Pyrene

Y. Oeda, O. Nishi, Y. Matsushima, K. Mizuno, A. H. Matsui, M. Takeshima and T. Goto

Materials Science and Engineering A , **217/218** (1996) 181-183.

6) Breakdown of the k Selection Rule and the ^1L_b Exciton Bandwidth in Pyrene Microcrystallites

Y. Oeda, O. Nishi, Y. Matsushima, K. Mizuno and A. H. Matsui

Proceedings of the Asia Symposium on Solid State Photophysics, 10-11 November 1995, Nara, (1995) 201-205.

7) New Technique to Determine Exciton Bandwidth of the Lowest Exciton Band in Aromatic Molecular Crystals
A. H. Matsui, O. Nishi, Y. Matsushima K. Mizuno, M. Takeshima, Y. Oeda, and T. Goto
Progress in Biomedical Optics, The Intl. Soc. for Optical Engineering, **2705** (1996) 103-109.

8) Exciton Bandwidths of the Lowest Exciton Band in Anthracene and Pyrene Crystals
A. H. Matsui, K. Mizuno, M. Takeshima, Y. Oeda, and T. Goto
Proceedings of the 2nd International Conference on Excitonic Processes in Condensed Matter, August 14-17 (1996) 247-250.

9) Size Dependence of Exciton Bandwidth and Exciton Surface Scattering at Microcrystallite Surface Region
Y. Oeda, K. Mizuno and A. M. Matsui
Proceedings of The 2nd Asia Symposium on Condensed Matter Photophysics 1-2 November 1996, Nara (1996) 29-32.

10) Exciton Scattering, k Selection Rule, Exciton Bandwidth, in Pyrene Microcrystallites, and Lattice Relaxation Energy for the Origin of V Luminescence
Y. Oeda, O. Nishi, Y. Matsushima, K. Mizuno, A. H. Matsui,
M. Michinomae, M. Takeshima and T. Goto
Chem. Phys. **213** (1996) 421-427.

TABLE OF CONTENTS

1. INTRODUCTION

An exciton is a quasi particle observed in a variety of solids, such as ionic crystals, covalent crystals, and molecular crystals. A brief review of the history of excitons is presented here.

The original concept of the exciton was introduced by Frenkel in1931 [1] and then by Peierls (1932) [2] as a propagating quantum of elemental excitation in insulating crystals. Frenkel excitons are observed mostly in organic molecular crystals and described as a tightly-bound electron-hole pair. The subsequent quantum mechanical theory of Frenkel excitons was developed by Davydov (1948[3],1962[4]) who showed that the level splitting in electronic excited states occurs in crystal with translationally inequivalent molecules in a unit cell. The splitting at $k = 0$ is now known as the Davydov splitting. Prior to these theoretical works, Becquerel [5] first reported the absorption spectra of aromatic crystals in 1907 and subsequently experimental work on Frenkel excitons was done by many research groups [6-8] .

Besides these studies on Frenkel excitons, the optical study on Wannier excitons had also progressed in this period. The Wannier exciton (1937), which affords a clear contrast against the Frenkel exciton, has been recognized as a loosely-bound electron-hole pair[9]. The Wannier excitons are observed in various crystals such as copper oxide [10], alkali halides, heavy metal halides, semi-conductor materials and solid rare gases. The optical absorption spectra of alkali halides, which are currently understood as the Wannier exciton absorption spectra, were first reported by Hilsch and Pohl[11]. In the 1960's, excitonic processes such as translational motion, internal motion, two-photon absorption and coherent radiation were studied.

In the 1970's and later, interactions between exciton and other quasi particles were studied. The exciton-phonon interaction became the central topic among them and has been reviewed in several books [12-14]. Urbach [15] studied the absorption edge shapes of silver halides, and found that the absorption coefficient of AgCl varies exponentially with the incident photon energy. This empirical rule, now commonly known as the Urbach rule, was then studied theoretically by several groups [16-19]. The steepness parameter, σ, which appears in the Urbach rule, was interpreted to be directly related with the exciton-phonon coupling. According to Toyozawa [20], the magnitude of exciton-phonon coupling constant, g, provides an important criterion about the stability of self-trapped exciton state. A quantitative relationship between the steepness parameter, σ, and exciton-phonon coupling constant was then derived by Schreiber and Toyozawa [18]. The coupling constant $g = E_{LR}/B$, where E_{LR} is the lattice relaxation energy and B the exciton-band half width. After their work, the luminescence spectra of strong exciton-phonon coupled systems could be understood more quantitatively than ever before. The establishment of the Urbach rule has been confirmed in various aromatic molecular crystals [21-28].

The importance of the exciton bandwidth has recently been recognized more clearly, because the exciton bandwidth is an indispensable parameter in describing excitonic processes. It is therefore desirable to review the study of the exciton bandwidth here in detail. There are several useful parameters to describe excitonic properties, such as exciton energy levels, exciton bandwidth, exciton radius and so on. Among these parameters, the exciton bandwidth, $2B$, is an important parameter in characterizing, especially in describing dynamical behavior of excitons as mentioned before. However, for many years it was not

possible to determine the exciton bandwidth experimentally. The difficulty arises because the optical transition from the crystal ground state to $k \neq 0$ exciton states where k is the wave vector, is not allowed, because the optical transition from the ground state only to the $k = 0$ exciton state is allowed.

The problem was solved by Rashba [29], who suggested that the optical transition between the exciton band and a hot level of the ground state occurs independently of the wave vector k. This is based on the fact that the dispersion of the vibronic level of the ground state is negligible, say 2 to 3 cm^{-1}, then the absorption or luminescence spectrum due to the transition between the exciton band and the hot level of the ground state can provide the exciton bandwidth directly. Based on Rashba's idea several experimental works to find the exciton bandwidths were carried out. Robinson and his colleagues [30] measured the bandwidth of benzene and naphthalene crystals by a luminescence method, and Matsui et al. [31] determined the bandwidth of anthracene crystals applying a thermomodulation technique. However, as my earlier experiments had to be done at rather high temperatures, the results obtained involved some ambiguity caused by phonons. As I was involved in the latter work, I got interested in extending this work further.

Recently a novel technique which is applicable at lower temperatures has been developed [32]. In microcrystallites the wavevector k is not a good quantum number. Therefore, the optical transition from the ground state to the exciton band is allowed with all band states including $k = 0$ Fourier components of the exciton wavefunction and excitons at all band states are created. Thus the spectral width of the absorption spectrum thus obtained directly reflects the exciton bandwidth. The experiment can be done at low temperatures. From the observed bandwidth in microcrystallites, the exciton

bandwidth for bulk crystal is deduced as an asymptotic value.

We have applied this technique to pyrene microcrystallites. Pyrene is one of the well investigated materials of strong exciton-phonon interaction. The width of the lowest exciton band has been the subject of special interest to elucidate the exciton relaxation process associated with shallow self-trapped exciton luminescence. In a pyrene molecule, the lowest singlet excited state and the next higher singlet state are ^1L_b and ^1L_a states, respectively [33]. It has been discussed that the luminescence that originates from a shallow self-trapped state (V state) is associated with the ^1L_b band [34]. However, to discuss the V luminescence in detail the bandwidth of the ^1L_b band is required, which has never been explored experimentally for pyrene. Therefore the aim of this project is to determine the ^1L_b bandwidth and clarify exciton dynamics in pyrene crystal.

The excitonic states in pyrene along with the results obtained in this thesis are shown in Fig.1. The free exciton luminescence (named F luminescence), which appears at room temperature, is associated with the lowest narrow ^1L_b band as mentioned above, and the self trapped exciton luminescence (named S luminescence) is associated with the wide ^1L_a band. The present work thus provides additional information on excitonic processes.

We compare the exciton bandwidth data with those for anthracene microcrystallites and extend our work further. The recovery of the k selection rule in large microcrystallites was observed in both pyrene and anthracene at different microcrystallite sizes. In studying this problem has appeared another issue on exciton scattering at microcrystallite surfaces. We found it occurs strongly in anthracene microcrystallites and nothing in pyrene microcrystallites. This difference in the exciton scattering is interpreted in

terms of the high reactivity of anthracene molecules with PMMA used as solvent (environment) material to fabricate microcrystallites.

We will also discuss the spectral shape of the excitation spectra of pyrene and anthracene microcrystallites and level splitting within the exciton band.

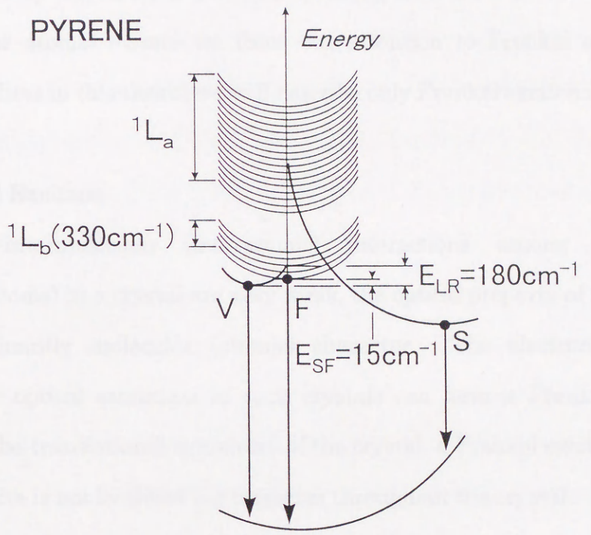

Fig.1 Schematic illustration of the adiabatic potential, whereby the F, S and V luminescence processes in pyrene bulk crystal are explained. The obtained values of ^1L_b exciton bandwidth, the lattice relaxation energy and the self-trap depth for the V state associated with ^1L_b band are shown: $2B$= 330 cm^{-1}, E_{LR}=180 cm^{-1} and E_{SF}=15 cm^{-1}.

2.FRENKEL EXCITONS IN MICROCRYSTALLITES

The Frenkel exciton and Wannier exciton offer two extreme models describing the collective excitation in non-metallic crystals. In addition, the charge transfer exciton is another model as an intermediate between these two models, whereby the electron and corresponding hole are located on different molecules (or atoms). Since we focus our attention to Frenkel excitons in microcrystallites in this thesis, we will describe only Frenkel excitons briefly.

2-1. Frenkel Excitons

When intermolecular (interatomic) interactions among individual molecules (atoms) in a crystal are very weak, the optical property of the crystal shows dominantly molecular (atomic) character. The electron-hole pair produced by optical excitation in such crystals can form a Frenkel exciton. Because of the translational symmetry of the crystal, a Frenkel exciton created at a lattice site is not localized but migrates throughout the crystal.

The excitation energy moves from one molecule (atom) to another as a wave in the crystal. For a crystal consisting of N unit cells and h molecules in each unit cell, the wavefunction of the excited state is obtained in a following way [4] :

$$\Phi_{\mu}^{f} = \left(\frac{h}{N}\right)^{1/2} \sum_{j=1}^{N} \exp\left(ik \cdot r_{j\mu}\right) \varphi_{j\mu}^{f} \quad , \tag{1}$$

where k is the wave vector describing the transfer of the excited energy and $\varphi_{j\mu}^{f}$ is the wavefunction of the f th excited state of the μ th molecule in the j th unit cell. Using Φ_{μ}^{f} , the wave function of the f th excited state of the crystal is written as

$$\Psi_i^f = h^{-1/2} \sum_{\mu=1}^{h} B_\mu^i \Phi_\mu^f \quad , \tag{2}$$

where B_μ^i is a coefficient of the molecule μ under the i th symmetry.

The electronic Hamiltonian, H_0 , of a crystal can be written as:

$$H_0 = \sum_{\mu=1}^{h} \sum_{j=1}^{N} H_{j\mu} + \sum_{j\mu \angle l\nu} V_{j\mu,l\nu} \quad , \tag{3}$$

where j and l refer to the unit sells, μ and ν to the lattice sites in the unit cell and $H_{j\mu}$ is the electronic Hamiltonian for the μ th molecule in the j th cell. $V_{j\mu,l\nu}$ is the interaction potential between molecules j μ and l ν. The eigenenergy value of an exciton with wavevector k is then obtained using Eq.(2) and Eq.(3) as:

$$E_f^p = E_f^0 + D_f + \sum_{l\nu} M_{l\nu,j\mu}^{f0} e^{ik(l\nu - j\mu)} \quad , \tag{4}$$

where p denotes the excited state symmetry, and E_f^0 is the excited energy of a free molecule. D_f is the site shift energy which is independent of the wavevector k. $M_{l\nu,j\mu}^{f0}$ is the matrix element of the excitation energy transfer from molecule l ν to molecule j μ , and it can be written as:

$$M_{l\nu,j\mu}^{f0} = \int \varphi_{l\nu}^{*0}(r_1) \varphi_{j\mu}^{*f}(r_2) V_{l\nu,j\mu} \varphi_{l\nu}^{f}(r_1) \varphi_{j\mu}^{0}(r_2) dr_1 dr_2 , \tag{5}$$

where $\varphi_{j\mu}^0$ and $\varphi_{j\mu}^f$ are wavefunctions of the ground and the f th excited state of the j μ th molecule, respectively. This matrix element gives a dipole-dipole interaction, under the assumption that the intermolecular overlapping of wavefunctions of excited states at different sites is too small to use the Heitler-London model. Thus the propagation of a Frenkel exciton in its notion is caused essentially by the dipole-dipole interaction.

The excitonic state in a bulk crystal is schematically shown in Fig.2. The left diagram shows the optical transition in a free molecule with the excitation energy E_f^0. When molecules aggregate to form a crystal, the intermolecular interaction reduces the electronic energy. Since the energy reduction in the excited state is not equal to that occurs in the ground state, the optical transition energy of a molecule E_f^0 shifts by D_f. The shift is thus called the site shift energy and it is negative, as shown in Fig. 2, where the excited state has N fold degeneracy. In a crystal, however, the degeneracy is lifted to form a band. On the right hand diagram the band thus formed is depicted as a shaded zone (Fig. 2).

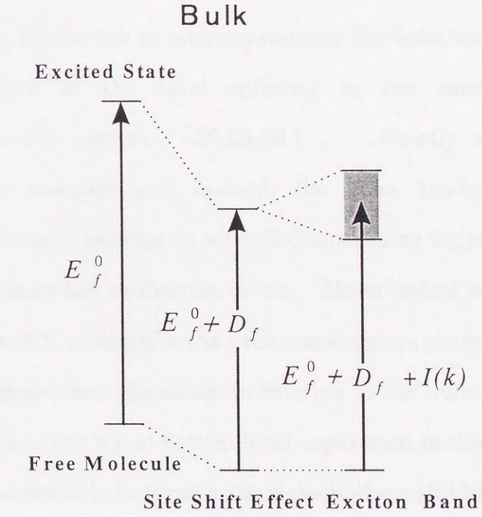

Fig.2 Schematic illustration of excitonic states in bulk crystal together with electronic states of a free molecule.

2-2. Exciton Bandwidth in Bulk Crystals

Molecular crystals are composed of molecules which are bound by the van der Waals interaction. The intermolecular interaction is very weak compared to the intramolecular interaction. Therefore, the excited states in molecular crystals are primarily localized at each molecular site and extended to only a small region, and the resulting exciton bandwidth is anticipated to be small so that the exciton motion in a crystal is very sensitive to trapping and scattering. We emphasize here again that the determination of the exciton bandwidth is especially important to discuss dynamical behavior of excitons in a crystal.

2-3. Exciton Bandwidth in Microcrystallites

The term 'exciton bandwidth in microcrystallites' has been used referring to the maximum width of the level splitting in the excited state in microcrystallites in our papers [32,35-39]. Strictly speaking this terminology is not accurate and instead, the term 'top-to-bottom level separation' should be used because as we will discuss later the excited state of microcrystallites is described as discrete levels. Nevertheless we will use the word 'exciton bandwidth' to describe the excitonic states in microcrystallites in order to achieve a consistent discussion in relation to the bulk crystal. The exciton bandwidth, i.e., the top-to-bottom level separation in microcrystallites, increases from approximately half value, B, of the bulk-crystal bandwidth, $2B$, to nearly the full bulk value with increasing microcrystallite size.

Figure 3 shows schematically the optical excitations in a microcrystallites, together with those of a free molecule and a bulk crystal. The ground state is indicated by solid circles. On the left diagram, optical absorption in a free molecule is shown, where the excited state is just a point, giving the absorption

band as a sharp line. In a bulk crystal, the molecular level is broadened to form a band as we have discussed before. In direct-gap materials, the bottom level becomes the bottom state $k = 0$ in bulk crystal which is indicated on the right diagram. The exciton is characterized by the wavevector k out of which only

$k = 0$ is the final state of the optical transition from the ground state. The optical transitions to $k \neq 0$ states are not allowed. Therefore, the optical absorption spectrum in bulk crystal does not provide information on the exciton bandwidth.

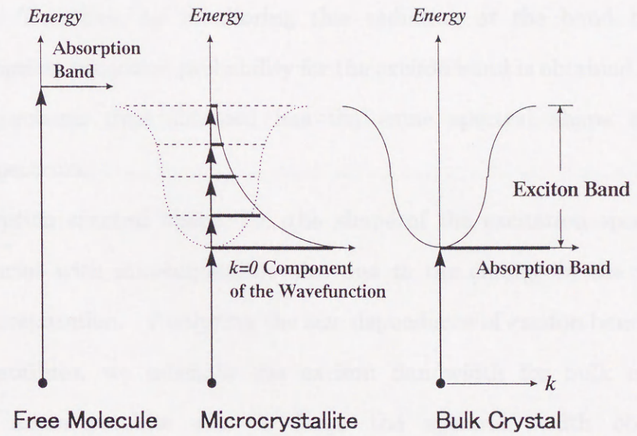

Fig.3 Optical excitations to a free molecule level (left), the exciton levels in a microcrystallite (center) and the bulk crystal exciton band (right). The absorption spectrum appears as a single sharp line spectrum in the free molecule as discrete lines. In the microcrystallite under confinement it appears as discrete lines. In the bulk crystal it appears as a single sharp line.

In microcrystallites, on the other hand, k is not a good quantum number since the presence of the boundary is especially important under a finite volume. The exciton wavefunction for a specific energy contains all k states, including the $k = 0$ component. Through this $k = 0$ component, the optical transition is allowed to all the levels of exciton band. Optical transitions are shown in the middle diagram by upward arrows. The intensity of the transition is indicated schematically by horizontal line length. The intensity is strongest at the bottom level but it decreases with increasing energy of the level. In microcrystallites as well as in bulk crystals, the photocreated excitons relax non-radiatively to the bottom state, from which the excitons recombine radiatively. Therefore, by monitoring this radiation at the band bottom energy, the optical transition probability for the exciton band is obtained. The excitation spectrum thus obtained has the same spectral shape as the absorption spectrum.

The absorption spectral shape, i.e., the shape of the excitation spectrum, naturally varies with microcrystallite size due to the change in the top-to-bottom level separation. Analyzing the size dependence of exciton bandwidth in microcrystallites, we estimate the exciton bandwidth for bulk crystal. When the microcrystallite size is large the spectral width obtained experimentally is almost equal to the bulk crystal bandwidth. Aromatic crystals such as anthracene and pyrene are particularly appropriate to study the exciton bandwidths, because the exciton absorption band in these crystals is located at an energy which is well separated from that of the band-to-band transition energy, and the oscillator strength for the band-to-band transition is weak. Thus we can determine the exciton bandwidth with less ambiguity.

3. EXPERIMENTAL

3-1. Character of Materials

Figure 4 shows the crystal structure of pyrene and anthracene. Their crystallographic properties, i.e. lattice constant, space group, density and molecular weight are summarized in Table 1[40]. The crystal structure of the pyrene belongs to the space group C_{2h}^5. Four molecules are involved in a unit cell. Two molecules located at each lattice site of the unit cell are oriented parallel to each other in a dimeric structure. The distance between these parallel molecules is 3.53 Å. This configuration allows overlap of the electron orbits between excited and unexcited molecules, giving strong interaction between them.

Anthracene is crystallized in a monoclinic form of a space group C_{2h}^5 with two molecules in a unit cell. The packing of molecules in the lattice of anthracene crystal differs from that of pyrene. One molecule at the corner of the unit cell (0,0,0) is translated to another molecules at (1/2,1/2,0) by a glide plane operation.

Material		Pyrene $C_{16}H_{10}$	Anthracene $C_{14}H_{10}$
Space Group		C_{2h}^5	C_{2h}^5
Lattice Constant	a (Å)	13.649	8.561
	b (Å)	9.259	6.036
	c (Å)	8.470	11.16
Angles between the axes of the unit cell β(°)		100.28	124.42
Molecular Weight (g/mol)		202.2	178.2
Density (g/m^3)		1.27	1.25
Number of molecules in the unit cell (h)		4	2

Table 1 Crystallographic data of anthracene and pyrene.

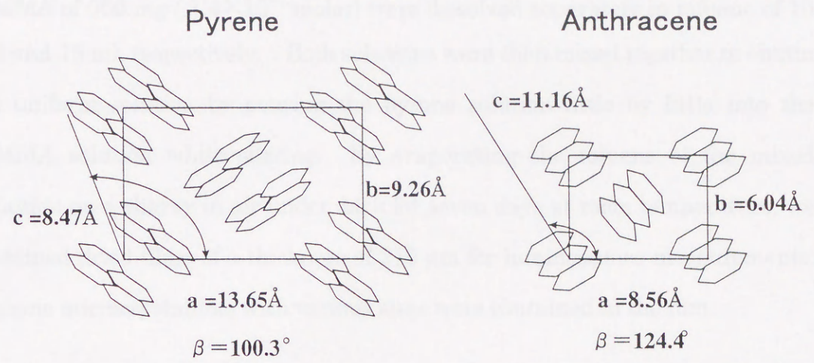

Fig.4 Structures of crystalline pyrene and anthracene showing the same space group C_{2h}^5. There are two molecules at each site in the unit cell of the pyrene crystal in contrast with one molecule at each site for the anthracene crystal.

3-2. Preparation of Specimens

Both pyrene and anthracene microcrystallites were embedded in poly (methyl-methacrylate) (PMMA : $(C_5H_8O_2)_n$ with n=7000～7500) [26]. PMMA does not have characteristic absorption bands in the spectral range from 360 to 1000 nm. Pyrene was purchased from a commercial source. It was first purified by chemical methods [41] and then by an extensive zone refining method. Purified pyrene powder of 9.6 mg (4.8×10^{-5} moles) and

PMMA of 950 mg (1.4×10^{-7} moles) were dissolved separately in toluene of 10 ml and 15 ml, respectively. Both solutions were then mixed together to obtain as uniform solution by pouring the pyrene solution little by little into the PMMA solution while stirring. By evaporating the toluene of the mixed solution on a sharay in air under dark for seven days at room temperature, we obtained dried films of a thickness of 215 μm for luminescence measurements. Pyrene microcrystallites with various sizes were contained in the film.

3-3. Optical System

Figure 5 shows our optical system used to measure the absorption, luminescence and excitation spectra. A 45 Watt halogen lamp was used as a light source to measure the absorption spectra. The light beam that is transmitted through two lenses, a collimator lens and a condenser lens, is focused on the specimen mounted on the cold finger of a cryostat and the transmitted light beam through the specimen was focused on the entrance slit of a SPEX/1403 double monochromator, which was equipped with a grating of 1800 grooves/mm to attain a high resolution. A slit width of 25 μ m applied corresponds to the spectral resolution of 0. 3 cm^{-1}. The signal detected by a photomultiplier was transferred to a home-computer through an AD converter.

The excitation spectra were obtained by illuminating the specimen with the light beam from a Xe lump, which was dispersed through a monocromator (NIKON/P-250; 1200 grooves/mm grating, spectral resolution for slit width 50 μ m is 15 cm^{-1}) . The reciprocal linear dispersion was 10 cm^{-1} at 19435 cm^{-1} (514.5 nm). A water filter was placed between two lenses L_5 and L_6 to absorb the IR light. The monochromator P250 for the exciting light system was driven by a stepping motor. The luminescence was monitored at the

backward scattering geometry. A used photomultiplier, R955 of Hamamatsu Photonics Inc., was cooled to obtain a higher signal-to-noise ratio. Luminescence spectra were obtained by the same arrangement as for measurements of the excitation spectrum. The specimen was immersed in liquid helium at 2 K.

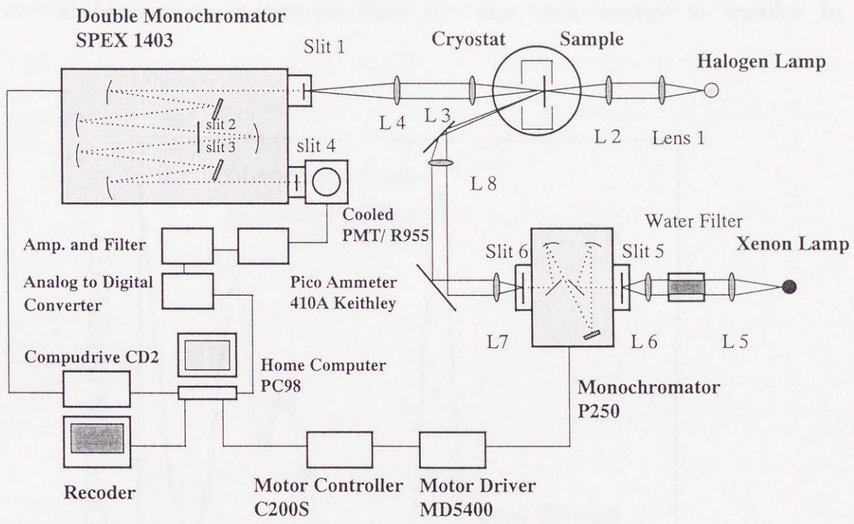

Fig.5 Optical system to measure the absorption, luminescence and excitation spectra of microcrystallites.

4. RESULTS

4-1. Absorption and Luminescence Spectra in Pyrene Microcrystallites

Figure 6 shows the absorption spectrum of pyrene microcrystallites embedded in PMMA at 2K. The 0-0 absorption peak position for bulk crystal is indicated with an arrow in the figure as reference. The 0-0 absorption bands of microcrystallites must be located at energies higher than that of bulk crystal because in microcrystallites the site shift energy is smaller in

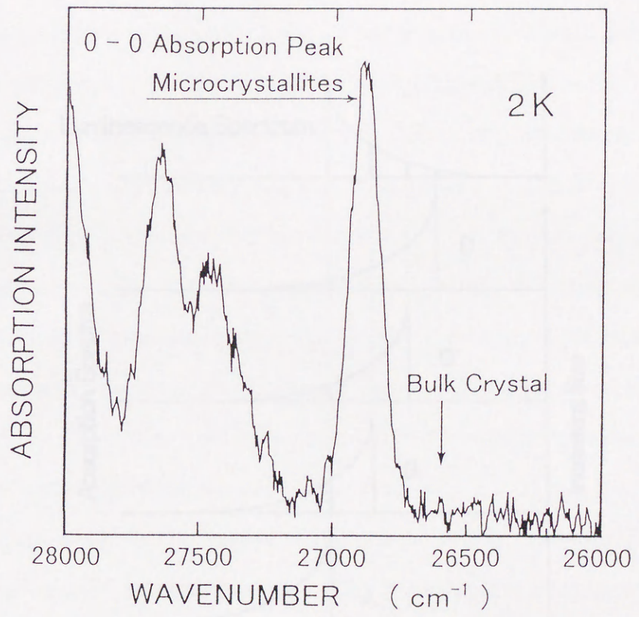

Fig.6 Absorption spectrum at 2 K of a pyrene microcrystallite specimen. The 0-0 peak position for pyrene bulk crystal is also shown with an arrow.

magnitude than in bulk crystal and the energy enhancement associated with the exciton confinement is expected. The lowest absorption band located around 26900 cm^{-1} is assigned to be the 0-0 band in microcrystallites, because it is located at energies higher than the bulk 0-0 band energy. The shape of the band is not sharp because our specimens include microcrystallites of various sizes, each of which gives the 0-0 absorption band located at a respective photon energy.

The luminescence spectrum provides direct evidence that our specimens contain microcrystallites of various sizes. Figure 7 illustrates how we can obtain a luminescence spectrum under illumination of a given photon energy.

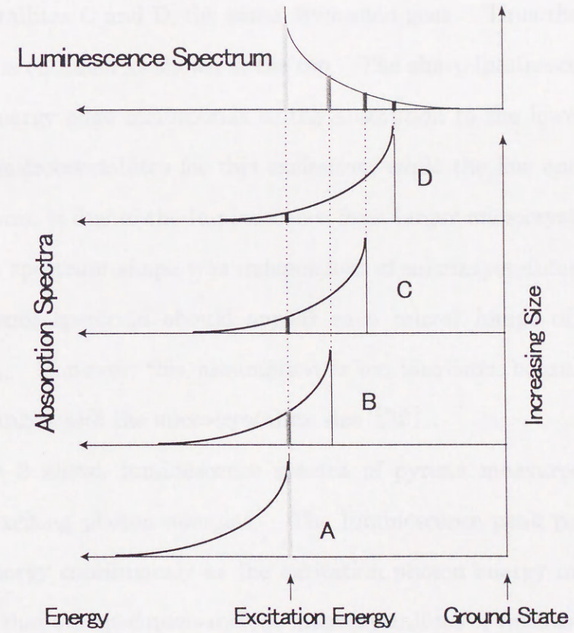

Fig.7 Schematic illustration of a luminescence spectrum for a specimen with various microcrystallite sizes.

The letters A, B, C and D, respectively, represent the absorption spectrum of microcrystallites, arranged in an increasing order of size from the bottom. Each absorption spectrum is equivalent to the excitation spectrum for the respective microcrystallite size. The intensity of the excitation spectrum indicates the magnitude of the $k = 0$ component of the wavefunction which was demonstrated in the middle diagram of Fig. 3. Under the excitation at the energy indicated in Fig. 7, microcrystallite A emits luminescence at the excitation photon energy because the excitation is done exactly at the bottom level of this microcrystallite. Microcrystallite B emits luminescence at a smaller photon energy than in microcrystallite A. The intensity of the luminescence is proportional to the intensity of the excitation spectrum. For microcrystallites C and D, the same discussion goes. Thus the luminescence spectrum is obtained as shown at the top. The sharp luminescence line at the highest energy edge corresponds to the absorption to the lowest level in the smallest microcrystallites for this excitation, while the low energy tail of the luminescence is due to the luminescence from larger microcrystallites. If the excitation spectrum shape was independent of microcrystallites size, then the luminescence spectrum should appear as a mirror image of the excitation spectrum. However, this assumption is too idealistic, because the spectral shape changes with the microcrystallite size [32] .

Figure 8 shows luminescence spectra of pyrene measured at 140 K at various exciting photon energies. The luminescence peak positions shift to higher energy continuously as the excitation photon energy increases. This indicates that our specimens include microcrystallites of various sizes.

The sharp line mentioned above and the exponential tail that follows the line are observed clearly at low temperatures. Figure 9 shows the

luminescence spectrum of pyrene microcrystallites measured at 2K. It demonstrates the presence of a combination of a sharp line and an exponential tail for every vibronic structure. We will not discuss here the assignment of these lines shown in the figure. The excitation photon energy is located exactly at a line position on the left edge. Since a filter was used to avoid the entry of an intense light to the photomultiplier the intensity of the spectrum at this photon energy appears weak.

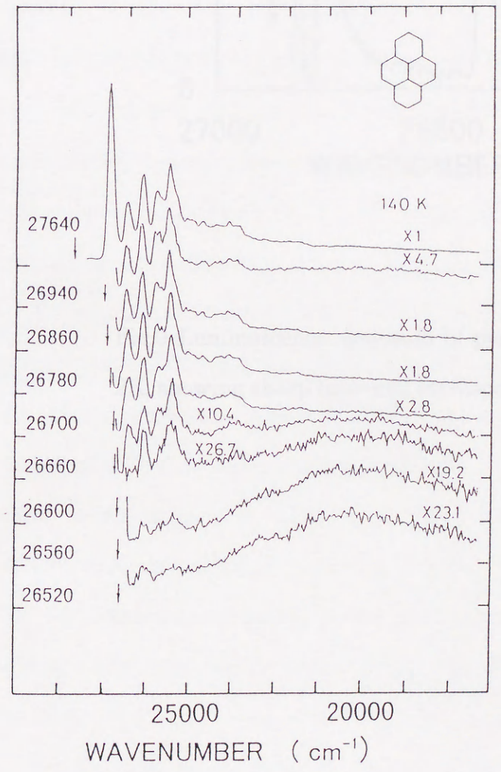

Fig.8 Luminescence spectra of pyrene microcrystallites under various exciting photon energies at 140 K. Vertical allows indicate the excitation photon energies and the relevant wavenumbers are shown on the left.

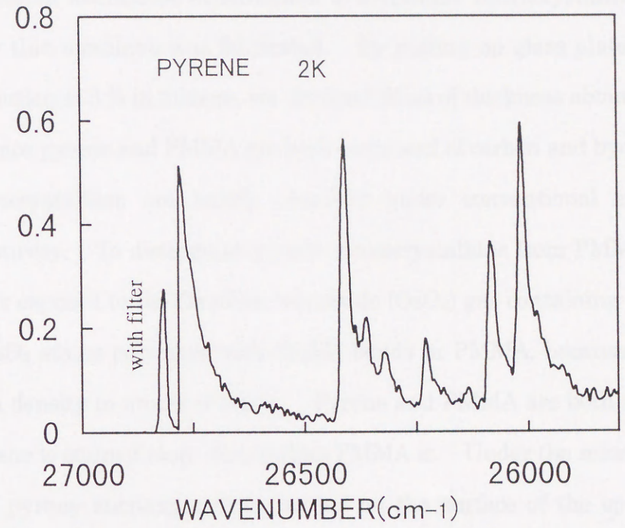

Fig.9 Luminescence spectrum of pyrene microcrystallites at 2K, showing sharp lines and corresponding exponential tails.

4-2. Microcrystallite Size

For an electron microscope examination to determine microcrystallite sizes an extremely thin specimen was fabricated. By pulling up glass plates from the mixed solution of 3 % in toluene, we obtained films of thickness about 600 Å [42]. Since pyrene and PMMA are both composed of carbon and hydrogen, pyrene microcrystallites are hardly observed under conventional electron microscopic survey. To distinguish pyrene microcrystallites from PMMA, the specimen was exposed to the Osmium tetraoxide (OsO_4) gas containing dye for a week. OsO_4 stains polymers with double bonds in PMMA, because of the high electron density in atoms of OsO_4. Pyrene and PMMA are both stained gray but pyrene is stained more deeply than PMMA is. Under the microscopic examination pyrene microcrystallites located on the surface of the specimen was evaporated by the heat due to the electron beam. The microcrystallite prints thus left on the specimen facilitate size measurements.

We measured the length and width of each print on an electron microscope photograph. About two hundred microcrystallite prints were examined under 4×10^5 magnification. The average value of the length and width for each microcrystallite is taken as the particle size. The largest and smallest particle sizes thus found were 47 Å and 18 Å, respectively. The particle size distribution histogram is shown in Fig.10. The histogram of particle size distribution is approximated by a Gaussian function shown by a dashed curve, giving a good model of the distribution. The average particle size was found to be 32 Å.

The 0-0 absorption band of the specimen, shown in Fig. 6 can be also approximated by a Gaussian function. In view of the fact that the size distribution and 0-0 absorption band shapes are both Gaussian curves, we can

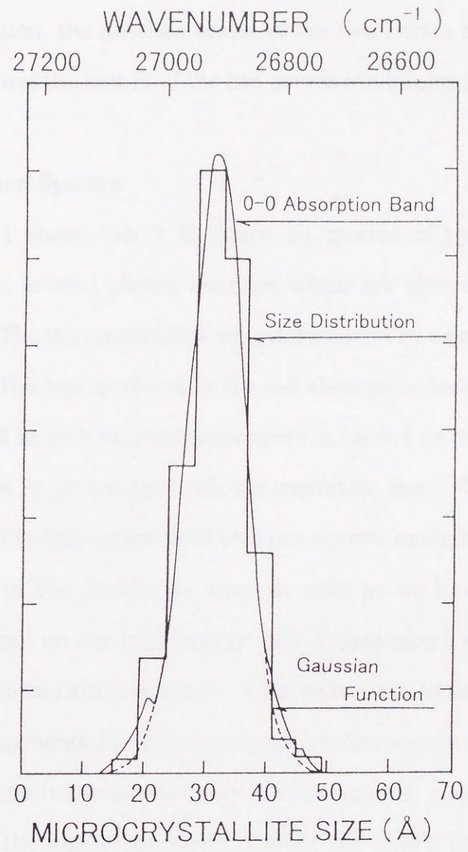

Fig.10 Particle size distribution histogram of pyrene microcrystallites in the specimen. The distribution is approximated by a Gaussian function (dashed line). The 0-0 absorption band (solid curve) is also approximated by a Gaussian function.

find one-to-one correspondence between a 0-0 luminescence energy and its microcrystallite size. In order to compare the 0-0 absorption band with the size distribution, the abscissa scales of the two curves have been altered and shifted so that the best fit of the two curves can be obtained.

4-3. Excitation Spectra

Figure 11 shows the 2 K excitation spectra of pyrene microcrystallites monitored at several photon energies which are shown on the right of each spectrum. The microcrystallite sizes determined by using Fig.10 are shown in brackets. The top spectrum is the 0-0 absorption band as a reference. An intense band in each excitation spectrum is formed as the convolution of sharp luminescence lines together with the excitation line. The spectral resolution 30 cm^{-1} need in this experiment was not narrow enough to resolve each sharp line clearly in Fig. 11 but the lines do exist as we have seen in Fig. 9. In Fig.11, the tail on the high energy side of each sharp excitation band can be classified into two kinds of bands. One, referred to as component A, practically decreases exponentially with increasing photon energy (wavenumber). The exponential decrease appears very clearly on such a diagram as to show the ordinate in the logalithmic scale, though not shown here. Component A is particularly prominent in the spectra monitored at photon energies higher than 26830 cm^{-1}. The other referred to as component B appears as a broad band, overlapping with component A. Component B is clearly seen in some spectra , e.g., in the spectrum monitored at wavenumber 26700 cm^{-1} (size 52 Å).

Figure 12 shows the excitation spectra of anthracene microcrystallites for various sizes (19Å to 134Å) which were obtained at 2 K [38,39] . The shapes of the high energy tails for anthracene microcrystallites are very similar to

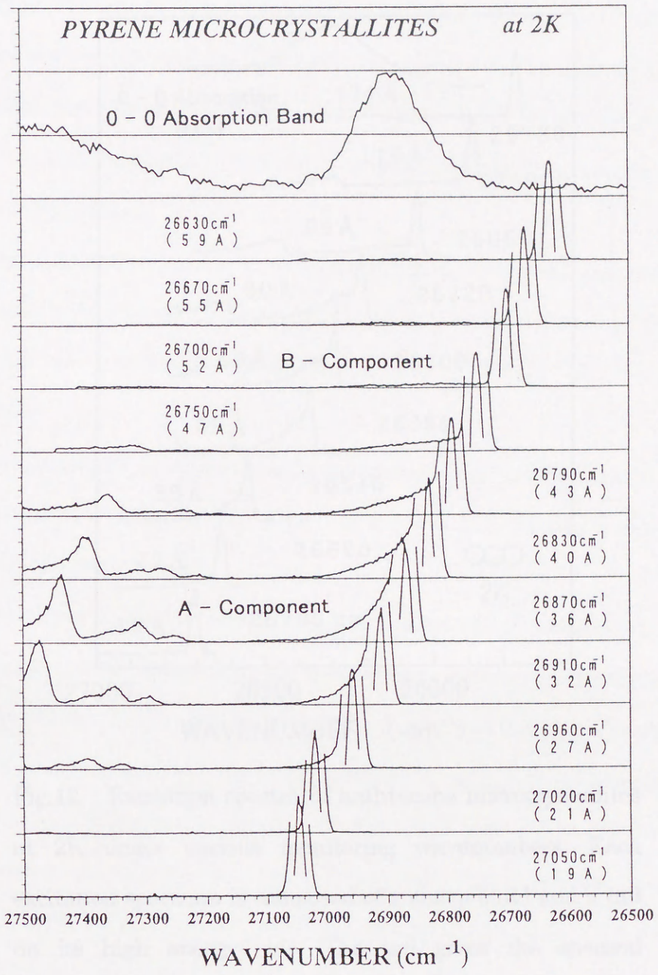

Fig.11 Excitation spectra of pyrene microcrystallites at 2 K under various monitoring wavenumbers. Each excitation spectrum is composed of a sharp band and a tail on its high energy side. The tail is composed of component A and component B; the former gives the exciton bandwidth of microcrystallites.

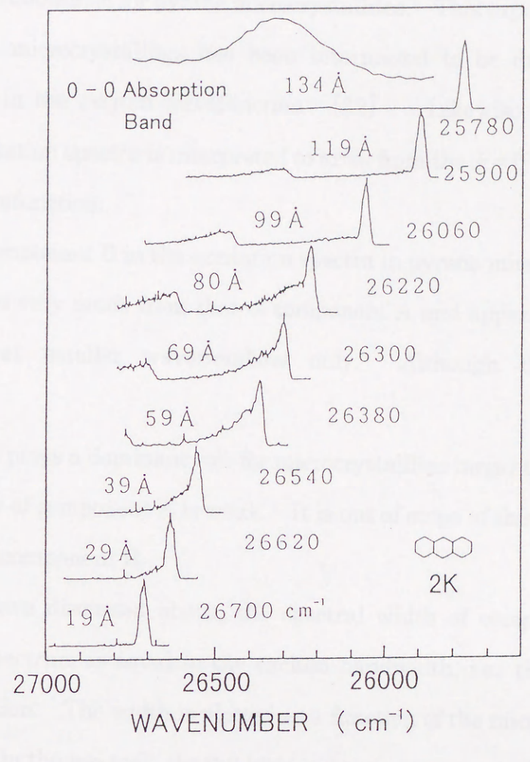

Fig.12 Excitation spectra of anthracene microcrystallites at 2K under various monitoring wavenumbers. Each excitation spectrum is composed of a sharp band and a tail on its high energy side. The tail gives the spectral bandwidth of anthracene microcrystallites.

component A obtained for pyrene microcrystallites. This exponential tail in anthracene microcrystallites has been interpreted to be due to the $k = 0$ component in the exciton wavefunction [32]. Likewise, component A in pyrene excitation spectra is interpreted to arise from the $k = 0$ component of the exciton wavefunction.

As for component B in the excitation spectra in pyrene microcrystallites, the shape differs very much from that of component A and appears in the spectra monitored at smaller wavenumbers only. Although the intensity of component

B is weak, it plays a dominant role for microcrystallites larger than 52 Å, where the intensity of component A is weak. It is out of scope of this thesis to clarify the origin of component B.

As we have discussed above, the spectral width of component A in the excitation spectrum is equal to the exciton bandwidth, i.e., the top-to-bottom level separation. The width is plotted as a function of the microcrystallite size in Fig.13. On the top scale the 0-0 luminescence energy, which corresponds to each microcrystallite size, is shown. In the small size region, the bandwidth goes to zero as the size goes to zero. This is quite reasonable because the size zero stands for a free pyrene molecule which should give only one sharp absorption line. For sizes 19 to 32 Å microcrystallites, the spectral bandwidth increases superlinearly with increasing size, and beyond this region the bandwidth approaches a maximum value of 330 cm^{-1}. For much larger microcrystallites, the bandwidth decreases rapidly to zero with increasing size.

Figure 14 shows the exciton bandwidth of the anthracene microcrystallites [39]. For anthracene microcrystallites, the exciton bandwidth increases linearly with increasing size for sizes 10 to 50 Å. Beyond this size region, the

bandwidth increases up to the maximum value 340 cm^{-1}, and then decreases asymptotically towards a constant value 300 cm^{-1}. For much larger microcrystallites, the bandwidth decreases rapidly torwards zero with increasing size as in the case of pyrene microcrystallites [38,39].

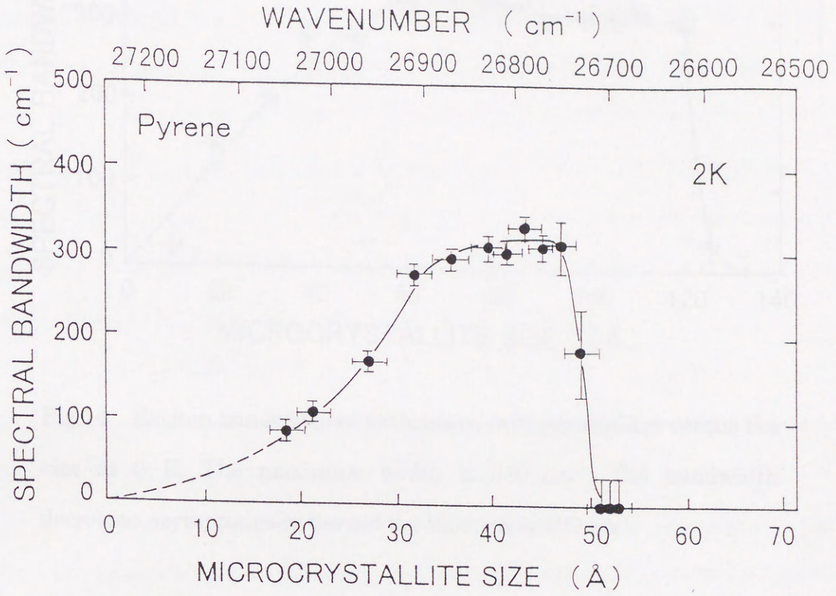

Fig.13 The bandwidth of the excitation spectra of pyrene microcrystallites plotted as a function of the microcrystallite size at 2 K. The maximum width is 330 cm^{-1}, which shows the exciton bandwidth in bulk crystal. The top scale indicates the photon energy of the sharp band to which the size is related.

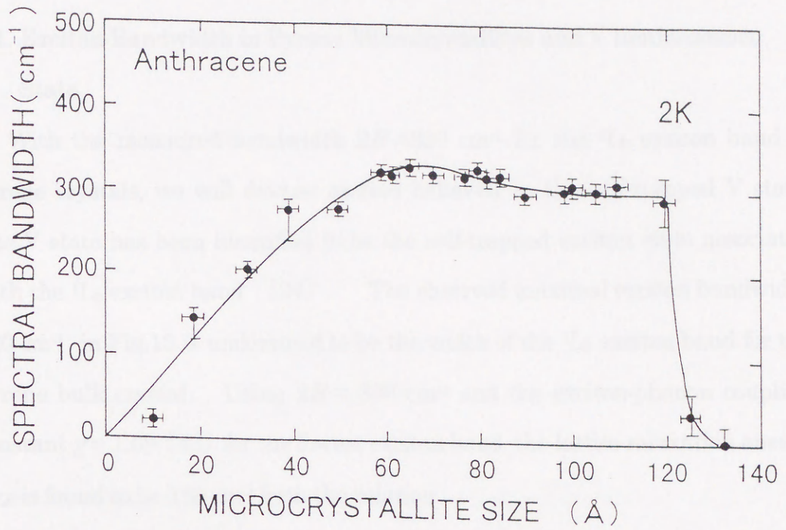

Fig.14 Exciton bandwidth of anthracene microcrystallites versus the size at 2 K. The maximum width is 340 cm^{-1}. The bandwidth decreases asymptotically toward the bulk value 300 cm^{-1}.

5. DISCUSSION

5-1. Exciton Bandwidth in Pyrene Microcrystallites and V luminescence State

With the measured bandwidth $2B$ =330 cm^{-1} for the ^1L_b exciton band of pyrene crystals, we will discuss exciton behavior in the self-trapped V state. The V state has been identified to be the self-trapped exciton state associated with the ^1L_b exciton band [34]. The observed maximal exciton bandwidth 330 cm^{-1} in Fig.13 is understood to be the width of the ^1L_b exciton band for the pyrene bulk crystal. Using $2B$ = 330 cm^{-1} and the exciton-phonon coupling constant g = 1.09 [43] for the lowest exciton band, the lattice relaxation energy E_{LR} is found to be 180 cm^{-1} from the relation

$$g = E_{LR} / B \qquad (6)$$

Thus the self-trap depth, $E_{SF} (= E_{LR} - B)$ for the V state is obtained to be 15 cm^{-1} as shown schematically in Fig.1.

Generally the bandwidth of the Frenkel exciton is comparable to the Davydov splitting. We will discuss the Davydov splitting in a crystal with two translationally equivalent molecule before we discuss the Davydov splitting in pyrene crystal where four translationally inequivalent molecules are involved.

In the crystal of having two molecules in the unit cell, the wavefunctions of the excited states in a crystal are given with Eq.(2) as

$$\Psi_1 = \frac{1}{\sqrt{2}}(\Phi_1 + \Phi_2) \quad , \qquad (7)$$

and

$$\Psi_2 = \frac{1}{\sqrt{2}}(\Phi_1 - \Phi_2) \quad . \qquad (8)$$

For wavefunctions Ψ_1 *and* Ψ_2 of the crystal, Eq.(4) is given as follows:

$$E_f^1 = E_f^0 + D_f + L_{11} + L_{12} \quad , \tag{9}$$

and

$$E_f^2 = E_f^0 + D_f + L_{11} - L_{12} \quad , \tag{10}$$

where

$$L_{11} = \sum_{n \neq 0} V_{0\alpha,n\alpha} e^{ikR} \quad , \tag{11}$$

and

$$L_{12} = \sum_{n,\alpha \neq \beta} V_{0\alpha,n\beta} e^{ikR} \quad , \tag{12}$$

Therefore, the exciton bandwidth $2B$ is obtained as

$$2\{ | L_{11} | + | L_{12} | \} \quad , \tag{13}$$

and the Davydov splitting, $E_j^1 - E_j^2$, is obtained as $2 | L_{12} |$. The exciton bandwidth is nearly the same or a little larger than the Davydov splitting because L_{11} is generally small compared to L_{12} in the case of a Frenkel exciton, which is shown schematically on the right hand side of Fig.15. In fact in bulk anthracene where two translationally inequivalent molecules occupy each unit cell the Davydov splitting is equal 220 cm^{-1} [44] and the exciton bandwidth is equal to 300 cm^{-1} [32] which is close to the value of the Davydov splitting as expected.

The Davydov splitting of the lowest exciton absorption band in pyrene crystal is about 15 cm^{-1} [45] as we have obtained and the exciton bandwidth is 330 cm^{-1}. This numerical controversy is possibly explained by considering the exciton wavefunctions in a crystal. In pyrene crystal, there are four molecules in a unit cell. Excited energy states of a crystal are split into four states which

are obtained using Eq.(2) as [45]

$$\Psi_1 = \frac{1}{2}(\Phi_1 + \Phi_2 + \Phi_3 + \Phi_4) \quad , \tag{14}$$

$$\Psi_2 = \frac{1}{2}(\Phi_1 - \Phi_2 - \Phi_3 + \Phi_4) \quad , \tag{15}$$

$$\Psi_3 = \frac{1}{2}(\Phi_1 + \Phi_2 - \Phi_3 - \Phi_4) \quad , \tag{16}$$

and

$$\Psi_4 = \frac{1}{2}(\Phi_1 - \Phi_2 + \Phi_3 - \Phi_4) \quad , \tag{17}$$

where $\Phi_1, \Phi_2, \Phi_3, \Phi_4$ are wavefunctions of excited states defined by Eq.(1). The transition to the ^1L_b state in pyrene from ground state is basically not allowed due to the unsuitable direction of the optical transition moment within the molecule. The optical transitions to the lowest ^1L_b state from the ground state are allowed for two excited states Ψ_2, Ψ_4 in the parity selection rule and the symmetry of crystal wavefunction. The four crystal wavefunctions $\Psi_1, \Psi_2, \Psi_3, \Psi_4$ belong to the irreducible representations Ag, Au, Bg and Bu, respectively. The character table for the C_{2h} factor group is shown in Table 2. In the last column the crystallographic direction of the polarization of the transition dipole is indicated. The optical transition to the states Au and Bu are allowed from the ground state and those to the states Ag and Bg are not allowed. The Davydov splitting, which is found as the energy difference between two optically allowed states, naturally does not show the maximal separation among those four states. The two Davydov states which are optically accessible from the ground states gives only a small splitting of 15 cm-

1. The exciton bandwidth 330cm^{-1} observed is much larger than the observed Davydov splitting but it is reasonable as explained mentioned above.

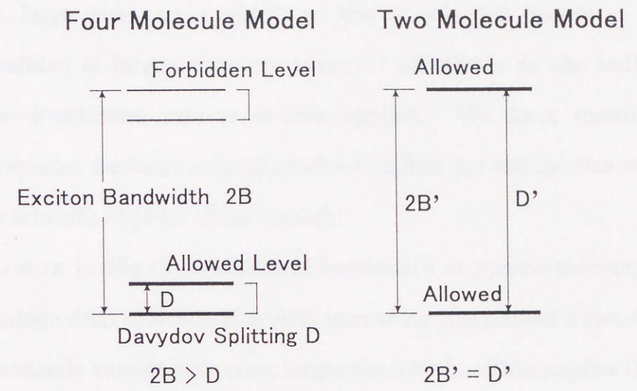

Fig.15 Illustration of the excitonic excited states and Davydov splitting at the case of four and two molecules in the unit cell.

C_{2h}	E	C_2^b	i	σ_b	
Ag	1	1	1	1	
Au	1	1	-1	-1	r_b
Bg	1	-1	1	-1	
Bu	1	-1	-1	1	r_a, r_c

Table 2 The irreducible representation of the C_{2h} factor group.

5-2. Recovery of the k Selection Rule

The excitation spectra obtained for the large size microcrystallites reflect the exciton bandwidth of bulk crystal. However the spectral bandwidth should vanish at large sizes as a result of the k selection recovery, i.e., the microcrystallites of larger sizes are regarded effectively as the bulk crystal where the k selection rule is strictly applied. We have measured the excitation spectra for large microcrystallites to find the critical size where the spectral bandwidth appears sharp enough.

As it is seen in Fig.13, the spectral bandwidth in pyrene microcrystallites shows a sudden drop to nearly zero with increasing size around a size 49 Å, and then it practically vanishes for sizes larger than 50 Å. This implies that the k selection rule which is lost for smaller microcrystallites is recovered. In other words, the exciton in microcrystallites larger than about 50 Å behaves like the bulk crystal exciton. Also, this fact offers a confirmation that the spectral bandwidths of the excitation spectra for microcrystallites truly represent the exciton bandwidth for bulk crystal at least in large microcrystallites. The critical size (50 Å) found above is consistent with the dipole lattice sum as will be discussed below.

The dipole lattice sum has been calculated in pyrene using the dipole approximation method [46] . The sum converges within 50 Å. This means that the minimum microcrystallite size at which from the view point of the exciton microcrystallites play an effective role of the bulk crystal is 50 Å. The critical size of 50 Å obtained from the discussion on the k selection rule agrees numerically with the value found by the dipole sum calculation.

Let us look at the critical size for anthracene. In Fig.14, the critical size for bulk to microcrystallite change is found to be 134 Å. On the other hand, the

dipole sum converges for anthracene within 75 Å [47] and does not agree with the critical size of 134 Å. This discrepancy gives us the estimation of the exciton surface scattering layer thickness (134 − 75)/2 Å(=30Å). We will discuss this issue in the next section.

5-3. Surface Scattering Layer

The traction of the surface layer volume to the total volume is sufficiently larger in microcrystallites than in bulk crystal. Thus in microcrystallites exciton surface scattering may appear prominently especially in smaller microcrystallites. In order to elucidate such scattering effect, we compare the bandwidth curve of pyrene microcrystallites shown in Fig.13 with that of anthracene microcrystallites in Fig.14. A remarkable difference between the microcrystallites of pyrene and anthracene is that the bandwidth of pyrene shows a monotonous increase with the microcrystallite size, reaching the bulk value, while in anthracene the width reaches the maximum value and then decreases toward the bulk value asymptotically [32]. The maximal width (340 cm^{-1}) which is larger than the exciton bandwidth in bulk crystal (300 cm^{-1}) by 40 cm^{-1} in anthracene. This extra width of 40 cm^{-1} has been attributed to the exciton scattering effect at microcrystallite surfaces [32].

We will discuss the origin of the exciton surface scattering. A possible origin for the scattering is some space charges at the interface between anthracene and PMMA as a solvent. Since the extra bandwidth (40 cm^{-1}) in anthracene has been attributed to exciton surface scattering and no such surplus width is found in pyrene microcrystallites, the surface scattering in pyrene must be negligible. In addition, in pyrene the bandwidth increases superlinearly in the small size region, while in anthracene it increases linearly.

These differences are consistent with the presence of surface scattering effect in anthracene microcrystallites predominant over that of pyrene microcrystallites.

Now, we have to elucidate the reason why exciton surface scattering occurs in anthracene microcrystallites but not in pyrene microcrystallites. Pyrene and anthracene crystals have practically the same ionization energies [48,49] and the same electron affinities [50,51].

The electron affinity of pyrene crystal is estimated to be 1.65 eV with ionization energy 5.75 eV and band gap energy 4.1 eV in ref. [50]. The value of 1.65 eve for the pyrene crystal is close to that for the anthracene crystal, 1.8 eV [50]. Therefore if charge transfer between pyrene and PMMA occurs, it must be in the same order as that between anthracene and PMMA. Consequently the exciton scattering effect due to the space charges is expected to be the same in both materials.

The experimental results do not agree with this suggestion. Instead, therefore, the presence of surface charge in anthracene microcrystallites is explained if one considers predominant reactivity of anthracene. According to the frontier electron theory [52], the highest reactivity in a molecule occurs at the point where the highest density of frontier electron exists. According to the calculation [52] the highest density in an anthracene molecule is by 40 % higher than that in a pyrene molecule so that anthracene is expected to be more reactive than in pyrene molecule by 40 %. As a result, the chemical reaction between anthracene and PMMA is considered to be much higher than that between pyrene and PMMA. Thus the scattering occurs strongly in anthracene microcrystallites. However it occurs only very weakly in pyrene microcrystallites since no chemical reaction between pyrene and PMMA is anticipated.

In the previous section we have suggested that the thickness of the exciton scattering surface layer in anthracene microcrystallites is 30 Å. A schematic illustration of the surface layer is shown in Fig.16.

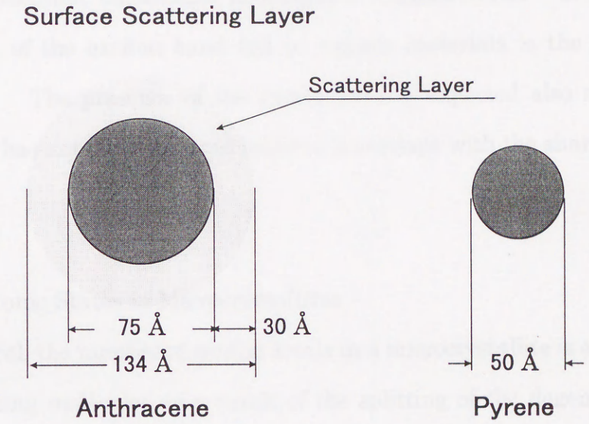

Fig.16 Schematic illustration of the surface scattering layer in anthracene and pyrene microcrystallites embedded in PMMA. Any surface scattering layer exists in pyrene microcrystallite.

5-4. Broadening of Spectral Bandwidth due to Surface Scattering Effect

As has been seen, for anthracene microcrystallites an excess bandwidth 40 cm^{-1} is observed. This excess value comes from the tailing of the exciton band at the top side. The similar tails due to the impurity scattering are well known at electronic band edges in inorganic semiconductors [53], but our observation of the exciton band tail in organic materials is the first to my knowledge. The presence of the excess band is expected also at the band bottom but has not been observed because it overlaps with the sharp intense 0-0 band.

5-5. Excitonic States in Microcrystallites

In general, the number of exciton levels in a microcrystallite is equal to that of constituting molecules as a result of the splitting of the degenerate states through molecule-molecule interaction. The discrete energy levels for small microcrystallites are described below. In Fig.17, the excited states in a microcrystallite is shown schematically based on a discrete level model. In microcrystallites, the site shift energy D_f is also negative as in Eq.(4) for bulk crystal and its absolute value increases with increasing size. In microcrystallites, exciton states are not specified by the wavevector k any more as we have discussed before but it is described by some discrete quantum numbers, n_x, n_y and n_z, as a result of the finite size. The exciton energy in microcrystallites can be written as

$$E(n_x,n_y,n_z) = E_m + D_f + I(n_x,n_y,n_z) \quad , \tag{18}$$

giving discrete energy states. In Eq.(18), the second term corresponds to the

site shift energy D_f in microcrystallites. The last term $I(n_x,n_y,n_z)$ represents the level splitting due to the intermolecular interaction. On the right in Fig.17, this energy splitting is shown by parallel lines.

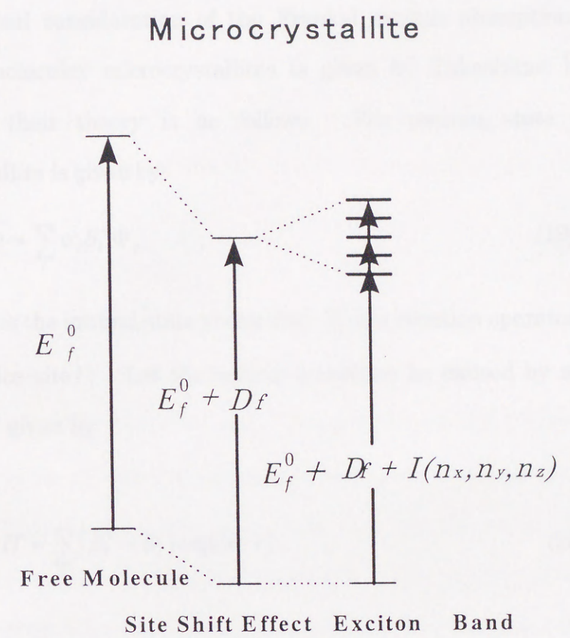

Fig.17 Schematic illustration of the exciton states in microcrystallites. The exciton energy in microcrystallites is not described by the wavevector k but some quantum number n.

In terms of the level splitting, we will proceed to discuss observed bandwidths for small microcrystallites: We are going to explain that the real bandwidth (top-to-bottom separation) in microcrystallites is much wider than the observed value.

Theoretical consideration of the Frenkel exciton absorption intensity in aromatic molecular microcrystallites is given by Takeshima [54] . The outline of their theory is as follows. The exciton state vector for a microcrystallite is given by

$$\Phi = \sum_l \alpha_l B_l^+ \Phi_g \quad , \tag{19}$$

where Φ_g is the ground state vector and B_l^+ is a creation operator of an exciton at the lattice site l . Let the optical transition be caused by a perturbation operator H' given by

$$H' = \sum_l \left(B_l^+ + B_l \right) \exp(i\kappa \cdot r) \quad , \tag{20}$$

where κ is the wavevector of the photon.

Using Eqs.(19) and (20), the transition matrix for the absorption is denoted as

$$\left\langle \Phi \left| H' \right| \Phi_g \right\rangle = \sum_l \exp(ikl) \alpha_l^* = S_k^* \quad . \tag{21}$$

Here we take approximately $\kappa = 0$ for photons. We assume that the transfer matrix element is non-zero only for the nearest neighbors and take the boundary condition that the transfer matrix is zero for the elements with either of the two lattices relevant to the matrix being outside the boundary. The optical transition rate $D(\theta_n)$ is, neglecting an unimportant multiplying

constant, given by

$$D(\theta_n) = \frac{2}{N+2} f(\theta_n) \quad , \tag{22}$$

where

$$\theta_n = \frac{n\pi}{N+2} \quad . \tag{23}$$

In the above equations, N is the number of lattice spacing, n is an odd number from 1 to N+1. $f(\theta_n)$ is defined as

$$f(\theta_n) = \left(\frac{\sin\theta_n}{1-\cos\theta_n} \right)^2 . \tag{24}$$

The energy E normalized over the half bandwidth B is given by

$$E(\theta_n) = 1 - \cos\theta_n \quad . \tag{25}$$

Figure 18 shows the calculated $f(\theta_n)$ as a function of $E(\theta_n)$, showing the shape of $D(\theta_n)$ [54] . This function gives the intense sharp line at n=1 and the exponential tail if N is large enough to give the separation of neighboring points smaller than the spectral resolution. The theory explains well the essential points of our excitation spectra which are composed of a sharp line followed by an exponential tail on the high energy side.

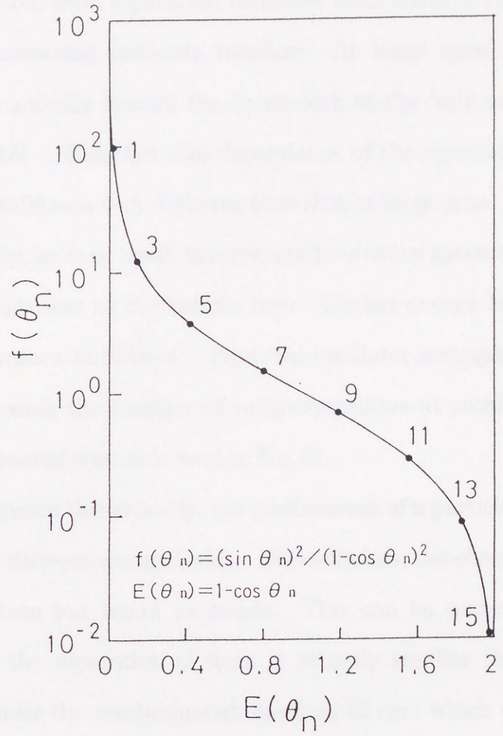

Fig.18 $f(\theta_n)$, which gives the transition rate $D(\theta_n)$ through Eq.(24), as a function of the normalized energy $E(\theta_n)$ assuming θ_n to be a continuous value. The points on the curve are for θ_n's for which states the transitions are allowed.

5-6. Size Dependence of Exciton Bandwidth

The top-to-bottom level separation increases from about B for a bimolecular particle with increasing molecule number. At large sizes the separation increases asymptotically toward the bandwidth of the bulk crystal $2B$ but never exceeds $2B$. Thus the size dependence of the spectral bandwidth in small microcrystallites is very different from that in large ones.

Experimentally, in very small microcrystallites every spectral band appears as a narrow single line as the bottom line. Higher energy lines are hard to detect for the reasons as follows. First, the oscillator strengths of such levels are small. Second, the number of microcrystallites at small sizes becomes small with decreasing size, as is seen in Fig.10.

As it is well known theoretically, the confinement of a particle within a small volume leads to discrete energy levels. Nevertheless, the observed spectra are not sharp as lines but broad as bands. This can be understood from the reasoning that the separation of lines is actually smaller than the spectral resolution. Under the resolutions as small as 12 cm^{-1} which we have applied as the narrowest slit width, it seems, though not sure, that the spectra consist of lines.

Thus the spectral bands may truly consist of lines. We should correctly talk of the top-to-bottom line separations, as was explained previously, instead of the spectral bandwidths but we will often talk of the latter because of the observed feature.

6. CONCLUSION

It has been shown that the microcrystallite technology offers a wide range of understanding of the Frenkel exciton behavior in bulk crystal through the study of exciton bandwidth. This technology also gives a new aspect of solution-solvent interface physics. The use of pyrene microcrystallites has played an important role in those studies by comparing with the results in anthracene microcrystallites. One of the main exciton problems in microcrystallites have thereby been solved and this has established a basis for further development of microcrystallite photophysics for which many interesting problems still remain, such as detailed exciton energy for various size of microcrystallites, discrete energy levels in small microcrystallites and the rapid decreasing of spectral bandwidths upon the k selection rule recovery.

REFERENCES

[1] J. Frenkel, Phys. Rev. 37 (1931) 17.

[2] R. E. Peierls, Ann. Phys. 13(5) (1932) 905.

[3] A. S. Davydov, J. Exptl. Theoret. Phys. (USSR) 18 (1948) 210.

[4] A. S. Davydov, *Theory of Molecular Excitons, McGraw-Hill, New York, (1962)p1.*

[5] Becquerel, Le radium 4 (1907) 328,through [8] p9.

[6] A. F. Prichotjko, J. Exptl. Theoret. Phys. (USSR) 19 (1949) 383.

[7] D. S. McClure and O. Schnepp, J. Chem. Phys. 23 (1955)1575.

[8] H. C. Wolf, *The Electronic Spectra of Aromatic Molecular Crystals, in*

Solid State Phys., vol. 9, ed. F. Seitz and D. Turnbull (Academic Press, New York, London, Tronto, Sydney, San Francisco, 1959) p1.

[9] G. H. Wannier, Phys. Rev. 52 (1937) 191.

[10] M. Hayashi and K. Katsuki, J. Phys. Soc. Japan 5 (1950) 380.

[11] R. Hilsch and R. W. Pohl, Z. Physik (1928) 384.

[12] M. Ueta, H. Kanzaki, K. Kobayashi, Y. Toyozawa and E. Hanamura , *Excitonic Processes in Solids,(Springer-Verlag, Berlin, Heidelberg, New York, Tokyo, 1994) p203.*

[13] K. S. Song and R. T. Williams, *Self-Trapped Excitons, (Springer-Verlag, Berlin Heidelberg New York, Paris, Hong Kong, Barcelona, Budapest, 1992) p300.*

[14] Jai Singh, *Excitation Energy Transfer Processes in Condensed Matter , Theory and Applications, (Plenum Press, New York and London,1994)p47,p111.*

[15] F. Urbach, Phys. Rev. 92 (1953) 1324.

[16] D.L. Dexter, Nuovo Cimento, Suppl. 7 (1958)245.

[17] H. Sumi and Y. Toyozawa, J. Phys. Soc. Japan 31(1971) 342.

[18] M. Schreiber and Y. Toyozawa, J. Phys. Soc. Japan 51 (1982) 1544.

[19] J. D. Dow and D. Redfield, Phys. Rev. B5 (1972) 594.

[20] Y. Toyozawa, *Exciton-lattice interaction-fluctuation, and defects formation, in vacuum Ultraviolet Radiation Physics, ed. E. E. Koch, R. Hansel, and C. Kunz, (Pergamon-Vieweg, Braunschweg, 1974) 317.*

[21] K. Tomioka, H. Amimoto, T. Tomotika and A. Matsui, J. Chem. Phys. 59 (1973) 4157.

[22] I. Nakada, J. Phys. Soc. Japan 20 (1965) 346.

[23] A. Matsui, J. Phys. Soc. Japan 21 (1966) 2212.

[24] K. Mizuno, A. Matsui and G. J. Sloan, J. Phys. Soc. Japan 53 (1984) 2799.

[25] A. Matsui and K. Mizuno, J. Phys. Soc. Japan 51 (1982) 3206.

[26] A. Matsui, K. Mizuno and M. Iemura, J. Phys. Soc. Japan 51 (1982) 1871.

[27] T. Yamamoto, S. Nakatani, T. Nakamura, K. Mizuno, A. H. Matsui, Akatsuka and H. Kawamura, Chem. Phys. 184 (1994) 247.

[28] K. Mizuno, J. Phys. Soc. Japan 59 (1990) 1458.

[29] E. I. Rashba, Soviet Phys. Solid State 5 (1963) 757.

[30] S. D. Colson, D. M. Hanson, R. Kopelman and G. W. Robinson, J. Chem. Phys. 48 (1968) 2215.

[31] A. Matsui, K. Tomioka, Y. Oeda and T. Tomotika, Surf. Sci. 37 (1973) 849.

[32] A. H. Matsui, K. Mizuno, O. Nishi, Y. Matsushima, M. Shimizu, T. Goto and M. Takeshima, Chem. Phys. 194 (1995) 167.

[33] T. Azumi, A. T. Armstrong and S. P. McGlynn, J. Chem. Phys. 41 (1964) 3839.

[34] K. Mizuno and A. Matsui, J. Lumi. 38 (1987) 323.

[35] Y. Oeda, O. Nishi, Y. Matsushima, K. Mizuno, A. H. Matsui, M. Takeshima and T. Goto, Materials Science and Engineering A 217/218 (1996) 181.

[36] Y. Oeda, O. Nishi, Y. Matsushima, K. Mizuno and A. H. Matsui, Proceeding of the Asia Symposium on Solid State Photophysics, 10-11 November 1995, Nara, (1995) 201.

[37] A. H. Matsui, O. Nishi, Y. Matsushima K. Mizuno, M. Takeshima, Y. Oeda, and T. Goto, Progress in Biomedical Optics, The Intl. Soc. for

Optical Engineering, 2705 (1996)103.

[38] A. H. Matsui, K. Mizuno, M. Takeshima, Y. Oeda, and T. Goto, Proceeding of The 2nd International Conference on Excitonic Processes in Condensed Matter, (1996) 247.

[39] Y. Oeda, O. Nishi, Y. Matsushima, K. Mizuno, A. H. Matsui, M. Michinomae, M. Takeshima and T. Goto, Chem. Phys. 213 (1996) 421.

[40] E. Schudt, G. Weits, *Strukturdaten organischer Kristalle band 5, Landolt- Bornstein, (Springer-Verlsg Berlin Heiderberg New York, 1971)p747,p832.*

[41] A. Matsui, M. Iemura and H. Nishimura, Memoirs of Konan Univ., Science Series 26 (1981) 1.

[42] K. Takahashi, thesis for the master degree at graduate school of Konan Univ. 1993.

[43] A. Matsui and K. Mizuno, J. Phys. Soc. Japan 51 (1982) 3206.

[44] M. S. Brodin and S. V. Marisova, Optika I Spektroskopiya 10 (1961) 473 through [4] p84.

[45] D. P. Crag and S. H. Walmsley, *Excitons in Molecular Crystals, Theory and Applications, (W. A. Benjamin, Inc, New-York, 1968) p38-48.*

[46] J. Tanaka, Bull. Chem. Soc. Japan 38 (1965) 86.

[47] A. Matsui and Y. Ishii, J. Phys. Soc. Japan 23 (1967) 581.

[48] K. Seki, Mol. Cryst. Liq. Cryst. 171 (1989) 255.

[49] K. Seki, *Optical Techniques to Characterize Polymer Systems, e.d. H. Bassler,Elvevier Science, Amsterdam (1989) 151.*

[50] N. Karl, *Landolt - Boernstein, Numerical Data and Functional Relationships in Science and Technology, New Series, Eds. In chief K. H.*

Hellwege and O. Madelung, 17 Eds. O. Madelung, M. Shultz, and H.Weiss, p.106. Springer, Berlin, Heidelberg, New York, and Tokyo (1985).

[51] The electron affinity for pyrene crystal is estimated to be 1.65 eV with the ionization energy 5.75 eV and the band gap energy 4.1 eV in ref.50. This value 1.65 eV for pyrene crystal is close to that of anthracene crystal 1.8 eV.

[52] K. Fukui, T. Yonezawa and E. Shingu, J. Chem. Phys. **20** (1952)722.

[53] see for instance, E.O.Kane, Phys. Rev. **131** (1963)79 or G.D.Mahan and J. W. Conley, Appl. Phys. Letters 11 (1967) 29.

[54] M. Takeshima, A. H. Matsui, Chem. Phys. Letters **266** (1997) 135.

12

業 績 一 覧 表

尾枝芳隆

LIST OF PUBLICATION (Yoshitaka Oeda)

1) Exciton Band Structure of Crystalline Anthracene

A. Matsui, K. Tomioka, Y. Oeda and T. Tomotika

Surface Science, **37** (1973) 849-854.

2) Density of States and the Exciton Band Structure in Crystalline Anthracene

A. Matsui and Y. Oeda

Proceedings of the 6th Molecular Crystal Symposium, Klais (1973) 41-44.

3) An Experimental Approach to Determine the Density of States of an Exciton Band from Thermoabsorption Spectra

A. Matsui, K. Tomioka and Y. Oeda

Memories of Konan Univ. Science Series **16** (1973) 13-19.

4) Dynamical Behavior of Excitons in Crystalline Anthracene and Phenanthrene

K. Tomioka, A. Matsui, H. Amimoto and Y. Oeda

Memories of Konan Univ. Science Series **17** (1974) 1-22.

5) Densities of States of the ^1L_b Exciton Band and Luminescence Processes in Pyrene

Y. Oeda, O. Nishi, Y. Matsushima, K. Mizuno, A. H. Matsui, M. Takeshima and T. Goto

Materials Science and Engineering A , **217/218** (1996) 181-183.

6) Breakdown of the k Selection Rule and the ^1L_b Exciton Bandwidth in Pyrene Microcrystallites

Y. Oeda, O. Nishi, Y. Matsushima, K. Mizuno and A. H. Matsui
Proceedings of the Asia Symposium on Solid State Photophysics, 10-11 November 1995, Nara, (1995) 201-205.

7) New Technique to Determine Exciton Bandwidth of the Lowest Exciton Band in Aromatic Molecular Crystals
A. H. Matsui, O. Nishi, Y. Matsushima K. Mizuno, M. Takeshima, Y. Oeda, and T. Goto
Progress in Biomedical Optics, The Intl. Soc. for Optical Engineering, **2705** (1996) 103-109.

8) Exciton Densities of States and Exciton Bandwidth in Anthracene and Pyrene Microcrystallites
A. H. Matsui, K. Mizuno, M. Takeshima, Y. Oeda, and T. Goto
Proceedings of the 2nd International Conference on Excitonic Processes in Condensed Matter, August 14-17 (1996) 247-250.

9) Size Dependence of Exciton Bandwidth and Exciton Surface Scattering at Microcrystallite Surface Region
Y. Oeda, K. Mizuno and A. M. Matsui
Proceedings of The 2nd Asia Symposium on Condensed Matter Photophysics 1-2 November 1996, Nara (1996) 29-32.

10) Exciton Scattering, k Selection Rule, Exciton Bandwidth, in Pyrene Microcrystallites, and Lattice Relaxation Energy for the Origin of V Luminescence
Y. Oeda, O. Nishi, Y. Matsushima, K. Mizuno, A. H. Matsui,
M. Michinomae, M. Takeshima and T. Goto
Chem. Phys. **213** (1996) 421-427.